The Astronomical Journal, 134:604–616, 2007 August

CHEMICAL PROPERTIES OF STAR-FORMING DWARF GALAXIES

Ovidiu Vaduvescu
Instituto de Astronomía, Universidad Católica del Norte, Avenida Angamos 0610, Antofagasta, Chile; Former address: ACRU and SAAO, School of Mathematical Sciences, University of KwaZulu-Natal, Durban 4041, South Africa; ovidiuv@yahoo.com

Marshall L. McCall
Department of Physics and Astronomy, York University, 4700 Keele Street, Toronto, ON M3J 1P3, Canada; mccall@yorku.ca

and

Michael G. Richer
Observatorio Astrónomico Nacional, Instituto de Astronomia, Universidad Nacional Autónoma de México, P.O. Box 439027, San Diego, CA 92143-9027, USA; richer@astrosen.unam.mx
Received 2006 October 18; accepted 2007 April 14

ABSTRACT

Recent studies of the near-infrared (NIR) properties of dwarf irregular galaxies (dIs) and blue compact dwarfs (BCDs) have provided improved estimates for the NIR luminosity of old stellar populations in these galaxies. These can be used to derive gas fractions, and thereby to evaluate how BCDs have evolved with respect to dIs. Oxygen abundances have been derived for four BCDs in the Virgo Cluster from a run at Gemini-North in 2003. Combining these new abundances with published values, we study the correlations among the metallicity, K_s luminosity, gas mass, baryonic mass, and gas fraction. Within errors, the two types of dwarfs appear to share a common relation between the oxygen abundance and the luminosity in K_s. The correlation between metallicity and the gas fraction is the same for BCDs as for dIs, indicating that BCD evolution has been similar to that of dIs. Since dIs appear to have evolved as isolated systems, the BCD bursts are unlikely to be a consequence of gas infall or merging.

Key words: galaxies: abundances — galaxies: dwarf — galaxies: evolution — galaxies: formation — H II regions — infrared: galaxies — line: profiles

1. INTRODUCTION

1.1. *A Universe of Dwarfs*

Dwarf galaxies are by far the most numerous galaxies in the universe. About 80%–90% of the members of the Local Group are classified as dwarfs (Mateo 1998; Grebel 2001a), while about 85% of the known galaxies in the Local Volume ($D \lesssim 10$ Mpc) are also dwarfs (Karachentsev et al. 2004). The space density of dwarfs in the universe has been suggested to be about 40 times that of bright galaxies (Stavely-Smith et al. 1992).

Dwarf galaxies are defined arbitrarily as galaxies having an absolute magnitude fainter than $M_B \sim -16$ mag (Tammann 1994) or $M_V \sim -18$ mag (Grebel 2001a, 2001b). Based on their optical appearance, dwarf galaxies can be classified into five groups: dwarf irregulars (dIs), blue compact dwarfs (BCDs), dwarf ellipticals (dEs), dwarf spheroidals (dSphs), and dwarf spirals (dSs). The distinction between dEs and dSphs is not clear (e.g., Binggeli 1994), while dS's can be regarded as the very small end of spirals (Matthews & Gallagher 1997; Grebel 2001b). Excluding dSs, dIs and BCDs are the only systems harboring active or recent star formation activity. According to hierarchical clustering models of galaxy formation, larger galactic structures build up and grow through the accretion of dwarf galaxies (White & Frenk 1991; Kauffmann et al. 1993). Nevertheless, some recent evidence (e.g., Venn et al. 2004; Helmi et al. 2006) suggests that the halo of the Milky Way could not have been constructed from dSphs as we presently know them. In this picture, dIs and BCDs may be similar to the building blocks for more massive galaxies. As such, they are important probes for studying matter in its near-primordial state, thus being relevant to understanding galaxy formation and evolution.

Despite the advances in the last decades, the relation between dIs and BCDs remains unclear. Some authors suggest that BCDs and dIs are the same type of galaxy, with BCDs being dIs undergoing bursts of star formation (e.g., Thuan 1985). Others argue that dIs are a fundamentally distinct type from BCDs, with no simple evolutionary links between them (e.g., James 1994). Richer & McCall (1995) argued on chemical grounds that BCDs may be more akin to dSphs than dIs. Papaderos et al. (1996a) review previous arguments concerning the evolutionary relationships between BCDs, dIs, and dEs without reaching firm conclusions.

1.2. *Determining Chemical Abundances for Dwarfs*

The metallicity, Z, is defined as the fraction of elements other than hydrogen and helium by mass (e.g., Pagel 1997). Metallicity is a key parameter intimately linked to the formation and evolution of galaxies. It gives an indication of age in the sense that it reveals how far the conversion of gas into stars has proceeded. In practice, the metallicity in star-forming galaxies is quantified via the oxygen abundance, defined as the fraction of oxygen by number, $12 + \log [n(\mathrm{O})/n(\mathrm{H})]$. After hydrogen and helium, the most abundant element in the universe is oxygen. It is convenient to measure the oxygen abundance because it exhibits emission lines in H II region spectra which are very bright and easy to measure.

Physical and chemical properties of nebulae can be derived by measuring ratios of intensities of collisionally excited emission lines (e.g., Osterbrock 1989). Recombination lines of metals are normally too faint to detect in extragalactic nebulae, although in some of the very brightest objects recombination lines have been detected (e.g., Peimbert et al. 2007). The radiation emitted by a nebula depends on the abundances of the chemical elements and the physical state of the gas, especially its average temperature and density.

A natural reference for elemental abundances is the Sun, which has an oxygen abundance $12 + \log (\mathrm{O/H})_\odot = 8.69$ (e.g., Allende Prieto et al. 2001). We define $Z_\odot = (\mathrm{O/H})_\odot$. It is customary to

define "metal-poor" as a system with an abundance lower than this value, and "metal-rich" as a system with an abundance exceeding this value. The dIs and BCDs are the most metal-poor galaxies, having metallicities as low as $\sim 1/50\, Z_\odot$. In high-redshift clouds of gas, which may be building blocks of today's galaxies, the metallicity can reach values as low as $0.001\, Z_\odot$ (Kunth & Ostlin 2000). Stars in our Galaxy reach metallicities as low as $0.00001\, Z_\odot$ (Sparke & Gallagher 2000).

There are two commonly used methods to determine oxygen abundances in H II regions. The "direct method" (T_e) is founded on a direct measurement of temperature. It is applicable whenever the temperature diagnostic [O III] λ4363 is detectable and in which the doubly ionized O^{+2} ion represents the dominant form of oxygen (Osterbrock 1989). The most accurate oxygen abundances are derived using the direct method, but for most galaxies [O III] λ4363 is faint and difficult to detect. When [O III] λ4363 is not detected, the bright-line method (R_{23}), originally proposed by Pagel et al. (1979), is commonly used. The oxygen abundance is parameterized as a function of the ratio $R_{23} = (I[\text{O II}]\ \lambda 3727 + I[\text{O III}]\ \lambda\lambda 4959, 5007)/I(\text{H}\beta)$. Unfortunately, the R_{23} indicator is not a monotonic function of oxygen abundance; for a given value of R_{23}, two values of the oxygen abundance are possible. However, McGaugh (1991) suggested that $\log([\text{N II}]\ \lambda 6583/[\text{O II}]\ \lambda 3727)$ can be used as a discriminator between the lower and upper branches. To estimate oxygen abundances, we adopt the calibration of R_{23} developed by McGaugh (1994) which employs $O_{32} = I([\text{O III}]\ \lambda 4959, 5007)/I([\text{O II}]\ \lambda 3727)$ to discriminate between the two branches.

1.3. *Dwarfs and the Closed Box Model*

One of the simplest frameworks for galaxy evolution is the "closed box model" (Searle & Sargent 1972; Pagel 1997). According to this model, a galaxy consists initially of gas with no stars and no metals. The stellar initial mass function is assumed to be constant in time. Stars that end their life as supernovae are assumed to enrich the interstellar gas with metals immediately, thereby eliminating time as a variable. Throughout the entire time, the galaxy evolves as a closed system, with no mass inflow or outflow. For such a system, the metallicity at any given time is solely determined by the fraction of baryons which remains in gaseous form, which is referred to as the gas fraction.

Many researchers, starting with Lequeux et al. (1979), have examined how the metallicity of a galaxy depends on its mass or luminosity, finding that more massive galaxies are more abundant in metals. Skillman et al. (1989) confirmed a strong correlation between absolute magnitude and metallicity for local dIs, in the sense that the least luminous dIs are the most metal-poor systems. Richer & McCall (1995) derived a more robust L_B-Z relationship, based on a sample of 25 nearby irregular galaxies having well-determined and self-consistent distances, along with abundances calculated from measured [O III] temperatures. An enlarged sample was considered by Miller & Hodge (1996) with the same conclusions. The same correlation was found by van Zee et al. (1997) in another sample of 15 gas-rich, low surface brightness dwarfs.

Information about the chemical evolution of dwarf galaxies is buried within the L-Z relation, but it is extremely difficult to extract. This is because the relation is affected by both flows (which may influence the metallicity, but not the luminosity) and the detailed history of star formation (which affects both metallicity and luminosity). Luminosity is a proxy for stellar mass, but how representative of stellar mass it is depends on the bandpass.

In a series of four papers, Melbourne & Salzer (2002), Melbourne et al. (2004), Lee et al. (2004), and Salzer et al. (2005) studied the L-Z relationship of giant "starburst emission-line galaxies," using data in the visible and NIR. The authors derived a linear relationship with a steeper slope than previously found for dwarfs, finding that the slope decreases as the wavelength of the luminosity bandpass increases. Using spectra of 6387 emission-line star-forming galaxies, Lamareille et al. (2004) confirmed a linear L-Z relation in the local universe ($z < 0.15$) over a large range of abundances ($\sim$2 dex) and luminosities ($\sim$9 mag). Tremonti et al. (2004) used SDSS imaging and spectroscopy of about 53,000 star-forming galaxies at $z \sim 0.1$, finding linear L-Z relationships, although contours appear to level off at high luminosities ($M_g < -20$).

A more useful relation for studying chemical evolution is the correlation between metallicity and the gas fraction. Lee et al. (2003b, 2003c) used data in the visible to show that the oxygen abundance in dIs is tightly correlated with the gas fraction. The result was used to argue that dIs have evolved in isolation, without inflow or outflow of gas. The observations pointed to a subsolar yield (e.g., Garnett 2002), but the significance of this is difficult to assess because values for yields are critically dependent on methods used to determine abundances. However, yields are relative, being critically dependent on methods used to determine abundances. A somewhat different conclusion was reached by van Zee & Haynes (2006) who measured abundances in 21 apparently isolated dIs selected based on their morphological classification and distances determined mostly from systemic velocities. While several galaxies in their sample follow the closed box model, they argue that either outflow of enriched gas or inflow of pristine gas has occurred in most galaxies.

1.4. *NIR Imaging of Dwarfs*

The utility of light as a gauge of galaxy mass depends on the wavelength of observation. In star-forming galaxies such as dIs and most BCDs, the young population shines brightly in the visible, overwhelming the light from the old stellar component, which traces the bulk of the mass. Therefore, observations in the visible do not necessarily reflect the stellar mass of a galaxy. This problem can be reduced in the NIR, where the intermediate-age and old populations become more visible. Furthermore, light in the NIR is much less attenuated by extinction (absorption of light due to internal and Galactic dust) than light in the visible.

Vaduvescu et al. (2005, hereafter Paper I) and Vaduvescu et al. (2006, hereafter Paper II) studied the structural properties of dIs and BCDs in the NIR. The dI sample (Paper I) included 28 dwarfs from the Local Volume closer than 5 Mpc having accurate distances from the literature (i.e., derived using Cepheids and the tip of the red giant branch). The BCD sample (Paper II) included 16 dwarfs in the Virgo Cluster, all approximated to have the same distance modulus (DM = 30.62). The surface brightness profiles of dIs were fitted using a sech law, which models the light at all radii, while BCDs were fitted using a sech function to model the diffuse old component plus a Gaussian to model the young starburst (at small radii). Absolute sech magnitudes were derived using the known distances and correcting for the extinction. These data are used here to gauge the stellar masses of the systems and thereby make possible a detailed study of chemical evolution.

1.5. *The Present Paper*

In the present paper, we analyze the chemical properties of our dI and BCD samples. We use the NIR data gathered in Papers I and II, in conjunction with metallicities taken from the literature and derived from our own spectra, to derive fundamental relations relevant to the formation and evolution of dwarfs and to compare dIs and BCDs chemically.

TABLE 1
GEMINI-NORTH OBSERVING LOG

Galaxy (1)	α (2)	δ (3)	P.A. (deg) (4)	Date (UT) (5)	λ_c (Å) (6)	Exposure (No. exp × s) (7)
VCC 24	12 10 35.7	+11 45 38	147	2003 Mar 1	4680	3 × 600
	...	...	147	2003 Mar 1	5600	3 × 200
VCC 459	12 21 12.1	+17 38 21	111	2003 Mar 1	4680	3 × 600
	...	...	111	2003 Mar 1	5600	3 × 200
VCC 641	12 23 28.6	+05 48 59	15	2003 Mar 1	4680	3 × 600
	...	...	15	2003 Mar 1	5600	3 × 200
VCC 2033	12 46 04.5	+08 28 33	14	2003 Mar 2	4680	3 × 600
	...	...	14	2003 Mar 2	5600	3 × 200

NOTES.—Col. (1): Designation of galaxy in Virgo Cluster Catalog (VCC). Cols. (2) and (3): Right ascension and declination (J2000.0) for the center of the slit, where units of right ascension are hours, minutes, and seconds, and units of declination are degrees, arcminutes, and arcseconds. Col. (4): Slit position angle (east of north). Col. (5): Observing date. Col. (6): Central wavelength. Col. (7): Exposure time.

In § 2 we present spectral observations of four Virgo BCDs which we observed at Gemini North, and in § 3 their reduction. Sections 4 and 5 address chemical properties of dIs and BCDs, considering correlations among luminosity, metallicity, mass (in various forms), and the gas fraction. In § 6 we approach the implications for evolution, comparing dIs and BCDs in the context of the closed box model. Section 7 presents our conclusions.

2. GEMINI OBSERVATIONS

Using Gemini North with GMOS, we detected [O III] λ4363 in two of the four BCDs which we observed. Long-slit spectra of four BCDs in the Virgo Cluster (VCC 24, VCC 459, VCC 641, and VCC 2033) were acquired in queue mode on two nights between 2003 February 28 and March 2. The data were taken with the Gemini Multi-Object Spectrograph (GMOS) mounted at the f/15.82 focus of the Gemini North 8.1 m telescope located atop Mauna Kea, Hawaii. The slit width was 0.5″ and the slit length was 5.5′. The GMOS camera includes three CCDs with 2048 × 4608 pixels each, creating a mosaic of 6144 × 4608 pixels. Pixel sizes are 13.5 μm, so the scale is 0.0824″ pixel^{-1} along the dispersion axis and 0.0727″ pixel^{-1} along the slit axis. We used the B600_G5303 grating, which gave a spectral resolution of 0.45 Å pixel^{-1}. Data were acquired both in the blue (central wavelength of the grating 4680 Å, range 3298–6062 Å) and in the red (central wavelength 5600 Å, range 4218–6982 Å). Data were binned 4 × 4. Air masses were between 1.0 and 1.2, so the slit was not oriented along the parallactic angle.

Dome flat fields were acquired every night for all instrumental settings, interspersed between blue and red galaxy spectra, and also between blue and red standard star spectra. Biases were taken at the end of the run. One spectroscopic standard star, Feige 66, was observed once every night. We include the log of our observations in Table 1.

3. DATA ANALYSES

3.1. *Reductions*

Images were reduced using the GEMINI version 1.6 GMOS package under IRAF using the sequence given in Vaduvescu (2005). Bias and flat-field frames (the latter taken for each instrument setting) were applied first, then individual spectra were combined for each grating setting. The arc lamp spectra were corrected for bias and flat field and used to calibrate the combined red and blue spectra. The two-dimensional spectra were collapsed to one dimension. The same sequence was applied to the standard star spectra. Spectra were calibrated using the standard star observations, correcting for atmospheric extinction. The blue and red calibrated spectra were joined into final spectra, using the common lines Hβ λ4861, [O III] λ4959, and [O III] λ5007 to equalize flux scales. The scale factors ranged between 1.3 and 2.4.

Figures 1–3 present the reduced combined spectra of VCC 459, VCC 2033, VCC 24, and VCC 641. The first two are presented using different scalings to show the bright and faint lines. The last two show fewer lines, so they are displayed using a single scaling. In a few cases, a "fracture" due to imperfect combination of the red and blue spectra is visible in the overlapping region at 6200 Å. Because the scaling of the red and blue spectra was based entirely on emission-line fluxes, measurements of the emission lines should be unaffected.

3.2. *Line Measurements*

We detected [O III] λ4363 in the core of two Virgo BCDs, namely, VCC 459 and VCC 2033, for which it was possible to

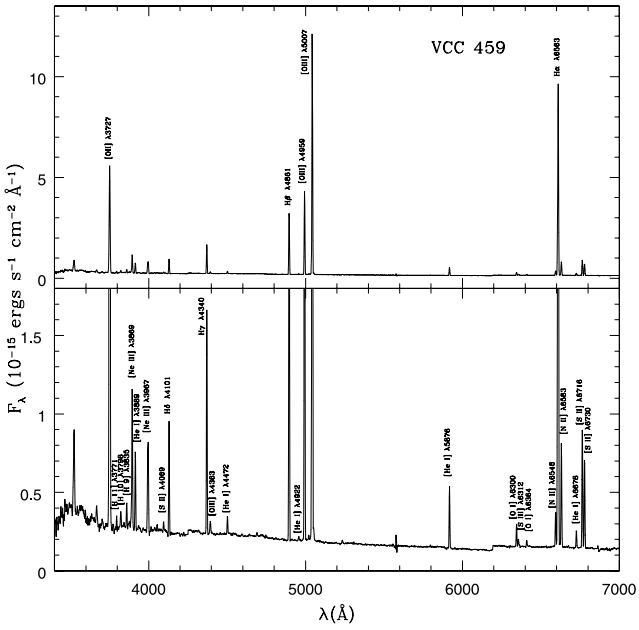

FIG. 1.—Reduced combined spectrum of VCC 459. For a better view of the lines, the spectra are shown at two vertical scalings. A "fracture" due to imperfect combination of the continua is visible at 6200 Å. This did not affect measurements of the emission lines.

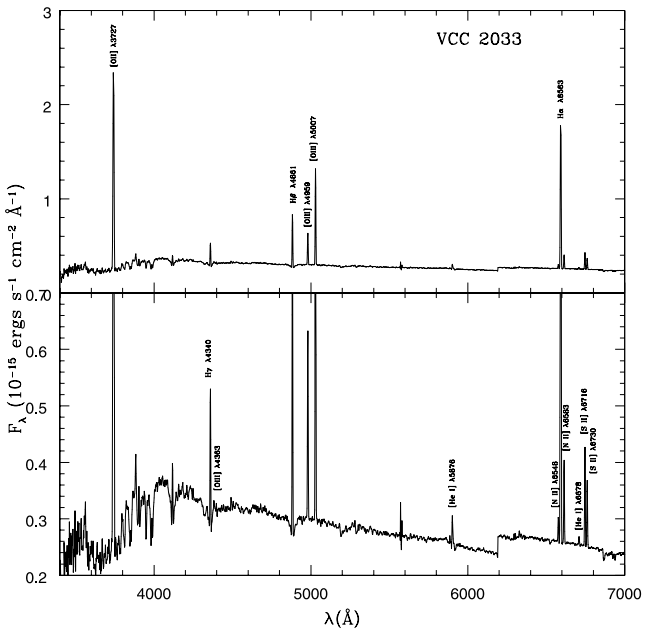

FIG. 2.—Reduced combined spectrum of VCC 2033. For a better view of the lines, the spectra are shown at two vertical scalings. A fracture due to imperfect combination of the continua is visible at 6200 Å. This did not affect measurements of the emission lines.

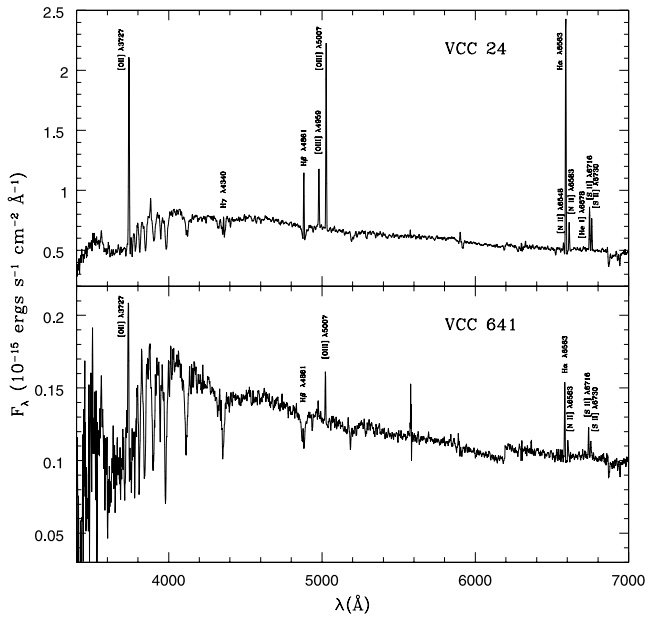

FIG. 3.—Reduced combined spectra of VCC 24 and VCC 641. A fracture due to imperfect combination of the continua of VCC 641 is visible at 6200 Å. This did not affect measurements of the emission lines.

determine the oxygen abundances using the direct method. In VCC 24 and VCC 641 we did not detect [O III] λ4363, but did measure stronger lines. For them, we were able to use the bright-line method to derive abundances.

Emission lines were measured using INTENS, a FORTRAN program developed by McCall et al. (1985). This is a noninteractive nonlinear least-squares fitting program which can efficiently fit and measure emission and/or absorption lines in one-dimensional spectra (flux vs. wavelength) or two-dimensional spectra (flux vs. wavelength as a function of spatial position). All spectra analyzed in this paper were one-dimensional.

A few of the hydrogen lines exhibited obvious underlying Balmer absorption, especially at Hβ. Using INTENS, a simultaneous fit of emission and absorption profiles allowed for a direct determination of the flux in the emission and the equivalent width of the underlying Balmer absorption. Measured emission fluxes are given in Table 2. In Figure 4 we illustrate two fits.

3.3. *Abundances*

We used SNAP (Spreadsheet Nebular Analysis Package; Krawchuk et al. 1997) to derive abundances from ratios of line fluxes. SNAP is an add-in for Microsoft Excel. From appropriately chosen spectral diagnostics, SNAP will compute reddening, apply equivalent width and reddening corrections, compute electron temperatures and densities, and compute ionic abundances.

Using SNAP, the extinction was calculated using the $F(\mathrm{H}\alpha)/F(\mathrm{H}\beta)$ ratio, assuming the reddening model of Fitzpatrick (1999) and that the dust is located in the Galactic foreground. The redshift of each galaxy was taken from NED. If the [O III] λ4363 line was detected, then the temperature was calculated using $I([\mathrm{O\ III}]\ \lambda5007)/I([\mathrm{O\ III}]\ \lambda4363)$. Otherwise, the temperature was assumed to be $T_e = 10{,}000$ K. The electron density was computed using the $I([\mathrm{S\ II}]\ \lambda6716)/I([\mathrm{S\ II}]\ \lambda6731)$ ratio. If the [S II] lines were poorly measured, a density of 100 electrons cm^{-3} was assumed.

Once the data were corrected for reddening, the ionic abundances of O^+ and O^{++} relative to H^+ were calculated for those objects for which [O III] λ4363 was detected. These were then summed to get $12 + \log [n(\mathrm{O})/n(\mathrm{H})]$.

We include in Table 2 the reddening-corrected line fluxes with respect to Hβ for VCC 24, VCC 459, and VCC 2033. For VCC 641, Hβ was severely affected by underlying absorption, so we report its line fluxes with respect to Hα instead.

Table 3 lists the measured chemical properties of the four BCDs observed. For VCC 2033, [O III] λ4363 was marginally detected, and thus, the oxygen abundance error is large (0.3 dex). Using the bright-line R_{23} method (McGaugh 1991, 1994), we derive $12 + \log(\mathrm{O/H}) = 8.31$, which is 0.3 dex higher than the [O III] λ4363 value [$12 + \log(\mathrm{O/H}) = 7.99 \pm 0.30$]. The R_{23} value seems to agree better with the measurement of Vilchez & Iglesias-Paramo (2003), who give lower and upper limits of 8.11 and 8.40, respectively. Due to the large error in our [O III] λ4363 measurement, we adopt for VCC 2033 an oxygen abundance which is the average value of the [O III] λ4363 and the R_{23} measurements, i.e., $12 + \log(\mathrm{O/H}) = 8.15 \pm 0.15$. For VCC 641, H$\beta$ was not detected, so in this case we used the emissivity calculations to determine the ratio Hα/Hβ, then we employed the bright line method. Van Zee et al. (2006) compare the reliability of empirical and semiempirical methods to derive abundances, suggesting that the typical error in an abundance derived from R_{23} is around 0.2 dex. We include this error for all our R_{23} results in Tables 3, 4, and 5.

4. CHEMICAL PROPERTIES OF DWARF GALAXIES

4.1. *Our Luminosity-Metallicity Relation for dIs*

In Table 4 we include the oxygen abundances for 17 dwarfs classified as dIs from our Local Volume sample, out of 27 observed in the NIR (Paper I), together with their sources. In the second part of the table we include four dwarfs from Virgo observed by us in the NIR (Paper II), classified as dIs based on their luminosity profiles. In the last part of the table we append another eight dIs with known metallicities from the literature for which K_s luminosities are determined from 2MASS data using the best distances available in the literature (R. Fingerhut 2005, personal communication). Note that 2MASS stars were used to derive zero points for

TABLE 2
OBSERVED AND CORRECTED LINE RATIOS

IDENTIFICATION (Å)	VCC 24[a]		VCC 459[a]		VCC 641[b]		VCC 2033[a]	
	F	*I*	*F*	*I*	*F*	*I*	*F*	*I*
[O II] λ3727	334.8 ± 16.1	344.8 ± 16.8	212.4 ± 1.4	230.2 ± 4.6	280.7 ± 48.2	297.3 ± 52.6	436.3 ± 4.4	447.0 ± 4.6
[H 12]	...	...	1.8 ± 1.2	2.0 ± 1.4	...	...	...	...
[H 11] λ3771	...	...	2.3 ± 0.3	2.5 ± 0.3	...	...	...	...
[H 10] λ3798	...	...	3.5 ± 0.3	3.8 ± 0.4	...	...	...	...
[He I] λ3820	...	...	0.6 ± 0.3	0.6 ± 0.3	...	...	...	...
[H 9] λ3835	...	...	4.3 ± 0.3	4.7 ± 0.4	...	...	...	...
[Ne III] λ3869	...	...	28.3 ± 0.6	30.3 ± 1.0	...	...	...	...
He I + H 8 λ3889	...	...	15.7 ± 0.5	16.9 ± 0.7	...	...	...	...
[Ne III] λ3967	...	...	20.2 ± 0.4	21.5 ± 0.6	...	...	...	...
[S II] λ4069	...	...	2.0 ± 0.3	2.1 ± 0.3	...	...	...	...
Hδ λ4101	...	...	22.3 ± 0.3	23.6 ± 0.6	...	...	...	...
Hγ λ4340	...	...	45.3 ± 0.4	47.1 ± 0.9	...	...	47.0 ± 2.0	47.5 ± 2.1
[O III] λ4363	...	...	2.8 ± 0.3	3.0 ± 0.4	...	...	2.1 ± 0.9	2.1 ± 0.9
[He I] λ4472	...	...	3.5 ± 0.1	3.6 ± 1.5	...	...	...	...
Hβ λ4861	100.0 ± 2.1	100.0 ± 4.3	100.0 ± 0.5	100.0 ± 1.0	...	...	100.0 ± 2.8	100.0 ± 3.0
He I λ4922	...	...	1.0 ± 0.4	1.0 ± 0.5	...	...	...	...
[O III] λ4959	92.2 ± 3.8	92.0 ± 4.0	132.3 ± 1.7	131.3 ± 2.3	54.9 ± 6.6	56.5 ± 7.3	57.8 ± 1.9	57.6 ± 2.0
[O III] λ5007	271.3 ± 8.0	270.2 ± 8.3	396.5 ± 2.0	392.1 ± 3.7	82.3 ± 11.5	84.5 ± 12.6	172.8 ± 3.8	172.2 ± 3.9
[He I] λ5876	...	...	12.4 ± 0.1	11.6 ± 0.1	13.8	13.9 ± 4.6 ± 0.5	9.0 ± 0.6	9.0 ± 0.7
[O I] λ6300	...	...	4.5 ± 0.1	4.2 ± 0.1	...	...	...	...
[S III] λ6312	...	...	1.6 ± 0.1	1.4 ± 0.1	...	...	...	...
[O I] λ6363	...	...	1.2 ± 0.1	1.1 ± 0.1	...	...	...	...
[N II] λ6548	16.8 ± 2.4	16.3 ± 2.5	7.5 ± 0.9	6.9 ± 0.8	...	...	7.6 ± 1.2	7.4 ± 1.3
Hα λ6563	373.9 ± 4.0	286.3 ± 4.4	314.6 ± 1.2	286.3 ± 0.6	100.0 ± 8.3	100.0 ± 9.1	261.4 ± 5.1	254.1 ± 5.3
[N II] λ6583	44.6 ± 2.8	43.1 ± 3.0	22.2 ± 0.9	20.2 ± 0.8	18.3 ± 3.3	18.3 ± 3.6	24.6 ± 1.4	23.9 ± 1.5
[He I] λ6678	4.6 ± 1.0	4.4 ± 1.0	3.6 ± 0.1	3.3 ± 0.1	...	...	2.6 ± 0.2	2.5 ± 0.2
[S II] λ6716	65.6 ± 2.5	63.2 ± 2.6	26.6 ± 0.1	24.1 ± 0.1	34.7 ± 3.6	34.6 ± 3.9	28.5 ± 0.6	27.6 ± 0.7
[S II] λ6730	50.0 ± 2.8	48.2 ± 3.0	19.4 ± 0.1	17.6 ± 0.1	21.3 ± 2.8	21.3 ± 3.1	19.7 ± 0.5	19.1 ± 0.5

[a] Flux ratios are reported with respect to Hβ (Hβ = 100).
[b] Flux ratios are reported with respect to Hα (Hα = 100). Wavelengths are listed in angstroms. *F* is the observed flux ratio. *I* is the flux ratio corrected for reddening.

our observed fields (Papers I and II), so the photometric scales are consistent. Nevertheless, one must be wary of 2MASS magnitudes for galaxies, owing to the short exposure times and the correspondingly bright detection thresholds.

In Figure 5 we plot the L_K-Z relationship for the 29 dIs in Table 4. For the galaxies observed by us, we use sech absolute magnitudes, while for the ones observed by 2MASS we use total absolute magnitudes. T_e-based abundances are plotted as filled symbols, and R_{23}-based abundances as open symbols. We include errors in metallicities; typical errors for absolute magnitudes are about 0.1 mag. There is an excellent correlation. Four outliers appear in the plot: NGC 5264 and NGC 3741, whose metallicities are derived using the bright line method, Holmberg II, whose K_s magnitude comes from 2MASS, and VCC 1725.

Following Lee et al. (2003b) a best-fit line for the correlation between two parameters with comparable errors can be obtained with the geometric mean functional relationship (Draper & Smith 1998, p. 89), which assumes similar dispersions in both observables. An equal weighting of points is assigned for both variables in a given fit. The geometric mean functional relationship relies on the minimization of the sum of areas bounded by the shortest horizontal and vertical lines from each data point to the best-fit line.

Excluding the four labeled points, we obtain the following L_K-Z relationship for 25 dIs from Table 4:

$$12 + \log(\mathrm{O/H}) = (-0.141 \pm 0.015) M_K + (5.581 \pm 0.244). \quad (1)$$

We plot the fit as a dashed line in Figure 5. Most of the points are consistent with the fit, given the errors in metallicities. A nearly identical relationship is obtained in *J*:

$$12 + \log(\mathrm{O/H}) = (-0.140 \pm 0.014) M_J + (5.692 \pm 0.214). \quad (2)$$

The rms dispersion in abundances in the L-Z relations in K_s and J is 0.11 and 0.10, respectively. Similar relations are obtained using the isophotal and total absolute magnitudes instead of the sech magnitudes.

4.2. *Our Luminosity-Metallicity Relation for BCDs*

In Table 5 we include 15 dwarfs classified as BCDs based on the literature and luminosity profiles. In the first part of the table, we include 12 BCDs from Virgo (Paper II), and in the last part we include the three dwarfs from the Local Volume classified as BCDs based on their luminosity profiles (Paper II) and van den Bergh (2000).

In Figure 6 we plot the L_K-Z relationship for 15 BCDs from Table 5. To sample the underlying stellar population, we employed sech magnitudes. T_e-based abundances are plotted as filled symbols, and R_{23}-based abundances as open triangles. We include errors in metallicities; typical errors for absolute magnitudes are about 0.1 mag. One outlier appears in the plot, VCC 641, having a very uncertain oxygen abundance. Excluding this point, we

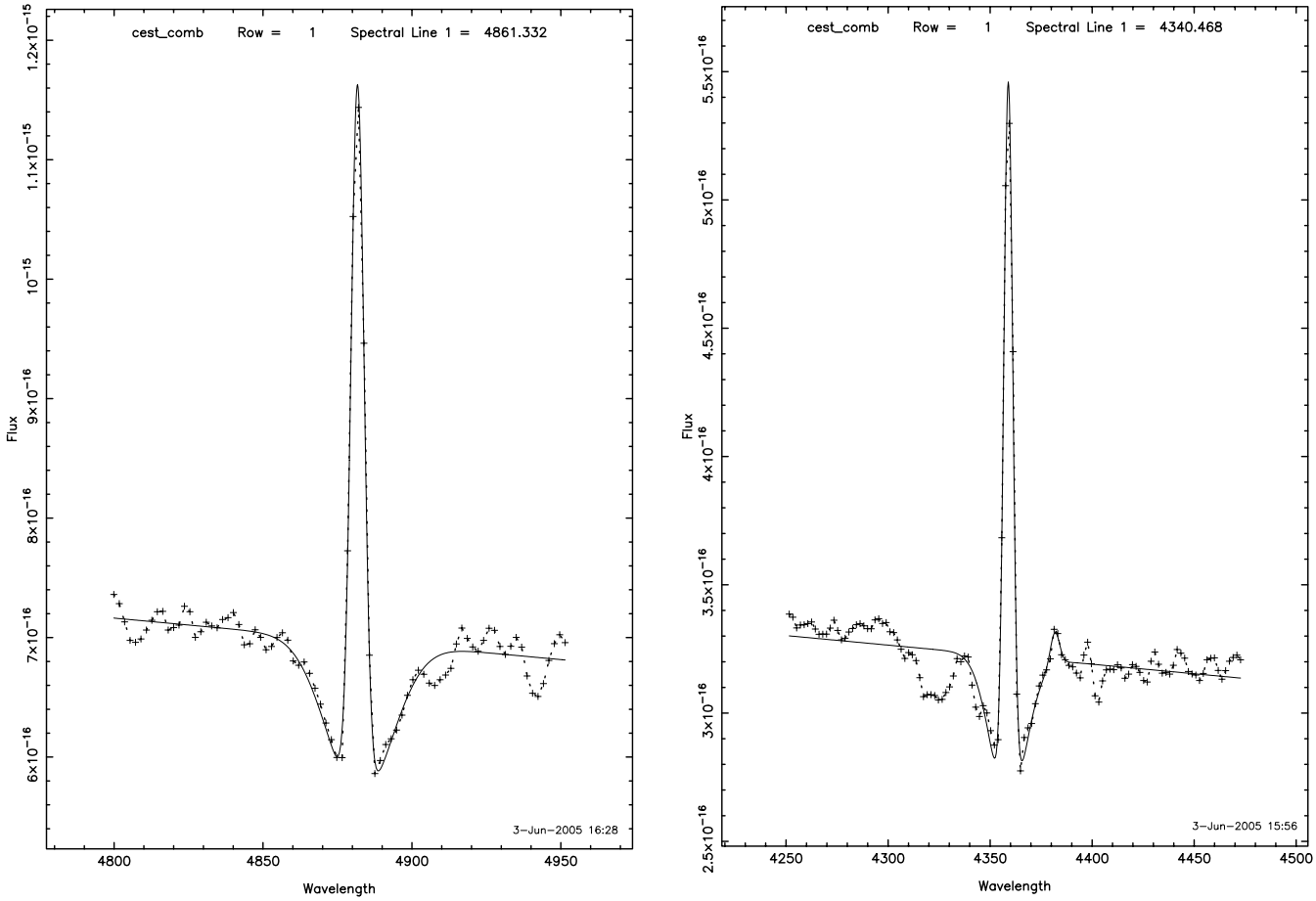

FIG. 4.—Flux vs. wavelength for two INTENS fits. *Left*: Hβ in VCC 24. *Right*: Hγ and [O III] λ4363 in VCC 2033. Plus signs mark observations, and solid curves are fits.

obtain the following L_K-Z relation for 14 BCDs from geometric mean fitting:

$$12 + \log(\mathrm{O/H}) = (-0.224 \pm 0.030)M_K + (4.212 \pm 0.537). \quad (3)$$

We plot the fit as a dashed line in Figure 6. A similar L_J-Z relationship is obtained in J:

$$12 + \log(\mathrm{O/H}) = (-0.216 \pm 0.028)M_J + (4.530 \pm 0.473). \quad (4)$$

The rms dispersion in abundance in the L-Z relations in K and J is 0.12 and 0.11, respectively. Similar relations are obtained using the isophotal and total magnitudes instead of the sech magnitudes.

In Figure 7 we combine the dIs and BCDs in our samples. For visibility reasons, we do not include the five outlier points. The solid line represents the L_K-Z relation for the dIs. Recall that the sech magnitude for BCDs excludes the luminosity of the starburst and so represents the underlying stellar component. Figure 7 illustrates that, although the L_K-Z relations for dIs and BCDs are formally different, the two samples largely overlap. Given the relatively poor luminosity distribution of our BCD sample (M_K

TABLE 3
DERIVED PROPERTIES FOR H II REGIONS IN VIRGO BCDS

Property	VCC 24	VCC 459	VCC 641	VCC 2033
$I(\mathrm{H}\beta)$ (ergs s^{-1} cm^{-2})	$(3.65 \pm 0.08) \times 10^{-15}$	$(2.38 \pm 0.07) \times 10^{-14}$	...	$(3.62 \pm 0.05) \times 10^{-15}$
τ_1	0.032	0.087	0.028	0.026
$W(\mathrm{H}\beta)$ (Å)	4.73 ± 0.10	92.80 ± 1.19	...	11.10 ± 0.17
n_e (cm^{-3})	...	52	...	...
$\log R_{23}$	0.849	0.877	1.097	0.830
$\log O_{32}$	0.021	2.273	−0.324	−0.289
$T_e(\mathrm{O}^{+2})$ (K)	...	10500	...	12500
$\mathrm{O}^+/\mathrm{H}^+$	...	$(6.9 \pm 1.4) \times 10^{-5}$	...	$(6.9 \pm 0.7) \times 10^{-5}$
$\mathrm{O}^{+2}/\mathrm{H}^+$	...	$(1.2 \pm 0.3) \times 10^{-4}$	...	$(2.9 \pm 1.3) \times 10^{-5}$
$12 + \log(\mathrm{O/H})[T_e]$	...	8.27 ± 0.09	...	7.99 ± 0.30
$12 + \log(\mathrm{O/H})[R_{23}]$	8.58 ± 0.20	8.09 ± 0.20	8.86 ± 0.20	8.31 ± 0.20

NOTES.—$I(\mathrm{H}\beta)$ represents the Hβ intensity, in ergs s^{-1} cm^{-2}, corrected for underlying Balmer absorption and reddening; τ_1 is the optical depth of dust at 1 μm, assuming a Fitzpatrick (1999) reddening model and dust in the foreground located in the Milky Way, calculated using Hα/Hβ; $W(\mathrm{H}\beta)$ is the emission equivalent width, in angstroms, corrected for underlying Balmer absorption; n_e is the electron density; $\log(R_{23})$ and $\log(O_{32})$ are the diagnostics for the bright-line method (Pagel et al. 1979, McGaugh 1994); $T_e(\mathrm{O}^{+2})$ is the computed electron temperature in kelvins; $12 + \log(\mathrm{O/H})[T_e]$ is the derived oxygen abundance in dex measured via T_e; and $12 + \log(\mathrm{O/H})[R_{23}]$ is the derived oxygen abundance in dex measured via R_{23}.

TABLE 4
PROPERTIES OF THE dI SAMPLE

Galaxy (1)	DM (2)	M_K (3)	$\log F_{21}$ (4)	$\log M_{\rm gas}$ (5)	$\log M_*$ (6)	μ (7)	$12 + \log$ (O/H) (8)	Method (9)	Reference (10)
Local Volume Sample									
Cas 1	27.59	−18.23	1.70	8.24	8.51	...	...	...	...
MB 1	27.59	−17.56	0.91	7.45	8.25	...	...	...	...
UGCA 92	26.20	−15.68	2.02	8.01	7.49	0.765	7.70 ± 0.20	R_{23}	HM95
Orion dwarf	28.66	−17.96	1.89	8.86	8.41	0.740	7.88 ± 0.20	R_{23}	LFM07
DDO 47	28.39	−15.04	1.88	8.74	7.24	0.970	7.85 ± 0.04	T_e	SKH89
UGC 4115	28.53	−16.60	1.32	8.24	7.86	0.704	7.81 ± 0.20	R_{23}	LFM07
DDO 53	27.58	−13.59	1.14	7.68	6.66	0.913	7.62 ± 0.05	T_e	SKH89
UGC 4483	27.37	−14.67	1.13	7.58	7.09	0.757	7.51 ± 0.03	T_e	STK94
UGC 4998	29.95	−18.53	...	...	...	...	...	...	...
UGC 5423	28.11	−16.17	0.58	7.33	7.69	0.304	7.98 ± 0.10	T_e	MH96
UGC 5692	27.83	−17.62	...	...	...	...	...	...	...
UGC 5848	29.70	−18.11	...	...	...	...	...	...	...
UGC 5979	30.55	−18.49	...	...	...	...	...	...	...
UGC 6456	28.03	−15.50	1.15	7.87	7.42	0.736	7.64 ± 0.10	T_e	TBD81
Mrk 178	27.78	−16.04	0.48	7.10	7.64	0.224	7.82 ± 0.06	T_e	GIT00
NGC 3741	27.24	−15.02	1.72	8.12	7.23	0.886	8.10 ± 0.20	R_{23}	GH89
NGC 4163	27.30	−16.34	0.98	7.41	7.76	...	...	...	...
NGC 4190	27.20	−16.47	1.37	7.76	7.81	...	...	...	...
Mrk 209	28.37	−15.67	1.00	7.85	7.49	0.698	7.77 ± 0.01	T_e	IT99
NGC 4789A	27.80	−15.63	2.16	8.79	7.47	0.953	7.67 ± 0.05	T_e	KS01
GR 8	26.52	−13.60	0.89	7.00	6.66	0.687	7.63 ± 0.10	T_e	MAM90
DDO 167	27.93	−14.56	0.66	7.34	7.05	0.662	7.66 ± 0.03	T_e	SKH89
UGC 8508	26.87	−15.43	1.15	7.40	7.39	0.506	7.89 ± 0.20	R_{23}	LFM07
NGC 5264	28.11	−18.64	1.09	7.84	8.68	0.127	8.64 ± 0.20	R_{23}	LGH03
Holmberg IV	29.22	−18.19	1.30	8.49	8.50	...	...	...	...
DDO 187	26.78	−14.33	1.08	7.30	6.95	0.688	7.69 ± 0.09	T_e	LMK03
Virgo Sample									
VCC 428	30.62	−15.78	−0.20	7.55	7.53	0.512	7.64 ± 0.09	T_e	VP03
VCC 1374	30.62	−18.17	0.40	8.15	8.49	0.315	8.35 ± 0.14	T_e	VP03
VCC 1699	30.62	−18.90	0.79	8.54	8.78	0.366	8.32 ± 0.06	T_e	VP03
VCC 1725	30.62	−18.81	0.28	8.03	8.75	0.162	7.74 ± 0.14	T_e	VP03
2MASS Sample									
NGC 55	25.94	−19.69	3.43	9.31	9.10	0.621	8.34 ± 0.10	T_e	WS83
NGC 1560	27.07	−18.25	2.65	8.98	8.52	0.743	> 7.97	T_e	LMK03
Holmberg II	27.50	−18.72	2.56	9.07	8.71	0.694	7.71 ± 0.13	T_e	LMK03
NGC 3109	25.72	−16.46	3.22	9.01	7.81	0.942	7.74 ± 0.33	T_e	LMK03
IC 2574	27.86	−17.15	2.65	9.30	8.08	0.943	8.09 ± 0.07	T_e	MH96
NGC 4214	28.25	−20.34	2.51	9.32	9.36	0.476	8.24 ± 0.12	T_e	KS96
NGC 5408	27.76	−16.39	1.81	8.42	7.78	0.814	8.01 ± 0.02	T_e	SCV86
NGC 6822	23.46	−16.83	3.38	8.27	7.95	0.674	8.11 ± 0.11	T_e	L05

NOTES.—Col. (1): Galaxy name, ordered by right ascension. Col. (2): Distance modulus. Col. (3): Absolute magnitude in K_s (sech for our sample, total for 2MASS). Col. (4): Logarithm of the total H I flux in Jy km s^{-1} (Karachentsev et al. 2004). Col. (5): Logarithm of the total gas mass in solar masses. Col. (6): Logarithm of the stellar mass in solar masses. Col. (7): Gas fraction. Col. (8): Oxygen abundance and uncertainty. Col. (9): Method of determining abundances: T_e, direct determination via [O III] λ4363 (Osterbrock 1989); R_{23}, determination via the bright line method (McGaugh 1994). Col. (10): Reference for abundance.

REFERENCES.—(KS97) Kobulnicky & Skillman 1997; (HM95) Hodge & Miller 1995; (LFM07) H. Lee et al. 2007, in preparation; (SKH89) Skillman et al. 1989; (STK94) Skillman et al. 1994; (MH96) Miller & Hodge 1996; (TBD81) Tully et al. 1981; (GIT00) Guseva et al. 2000; (M97) Martin 1997; (GH89) Gallagher & Hunter 1989; (IT89) Izotov & Thuan 1999; (KS01) Kennicutt & Skillman 2001; (MAM90) Moles et al. 1990; (LGH03) Lee et al. 2003a; (LMK03) Lee et al. 2003b; (WS83) Webster & Smith 1983; (KS96) Kobulnicky & Skillman 1996; (SKV86) Stasinska et al. 1986; (L05) H. Lee et al. 2005, private communication; (VP03) Vilchez & Iglesias-Paramo 2003.

mostly between −18 and −20), more data are required to definitively decide whether the two L_K-Z relations are really different.

4.3. *Comparison with the Literature*

In Table 6 we summarize different L-Z relationships presented in the literature. The L-Z relation we derive here for local dIs is similar to those found by others in the B band (Skillman et al. 1989; Richer & McCall 1995; Lee et al. 2003b; van Zee & Haynes 2006) and in the NIR (Saviane et al. 2005). The coefficients derived by us in the NIR are very close to the ones derived by Richer & McCall (1995) and van Zee & Haynes (2006) in the visible employing mostly T_e-based abundances. Using NIR luminosities has not reduced the scatter about this relation for dIs, perhaps due to the difficulty of obtaining sufficiently deep NIR photometry. Recently, Mendes de Oliveira et al. (2006) used data from Paper I and 2MASS to find a L_K-Z relation very similar to ours but with larger dispersion. Their sample includes 29 dwarfs, of which six appear to be BCDs. Lee et al. (2006a) find less scatter in the L-Z

TABLE 5
PROPERTIES OF THE BCD SAMPLE

Galaxy (1)	DM (2)	M_K (3)	log F_{21} (4)	log M_{gas} (5)	log M_* (6)	μ (7)	12 + log (O/H) (8)	Method (9)	Reference (10)
Virgo Observed Sample									
VCC 24	30.62	−17.54	0.58	8.33	8.24	0.553	8.27 ± 0.20	R_{23}	V05
VCC 144	30.62	−17.73	0.36	8.11	8.31	0.387	8.35 ± 0.07	T_e	VP03
VCC 213	30.62	−19.42	0.17	7.92	8.99	0.079	8.70 ± 0.20	R_{23}	VP03
VCC 324	30.62	−18.70	0.36	8.11	8.70	0.205	8.50 ± 0.10	R_{23}	VP03
VCC 334	30.62	−17.38	0.12	7.87	8.17	0.335	8.15 ± 0.05	R_{23}	VP03
VCC 459	30.62	−18.17	0.39	8.14	8.49	0.310	8.27 ± 0.09	T_e	V05
VCC 641	30.62	−17.25	0.05	7.81	8.12	0.325	8.86 ± 0.20	R_{23}	V05
VCC 802	30.62	−16.40	< −1.13	6.62	7.78	0.065	7.84 ± 0.15	T_e	VP03
VCC 848	30.62	−17.91	0.75	8.51	8.39	0.568	8.03 ± 0.16	T_e	VP03
VCC 1313	30.62	−15.07	0.01	7.76	7.25	0.765	7.77 ± 0.06	T_e	VP03
VCC 1437	30.62	−18.37	0.40	8.15	8.57	0.277	8.30 ± 0.20	R_{23}	VP03
VCC 2033	30.62	−17.91	−0.38	7.37	8.39	0.088	8.15 ± 0.15	$T_e + R_{23}$	V05
BCD Field Sample									
NGC 1569	26.37	−18.19	1.87	8.05	8.49	0.268	8.19 ± 0.04	T_e	KS97
NGC 3738	28.27	−18.59	1.34	8.28	8.64	0.305	8.23 ± 0.01	T_e	M97
IC 10	24.35	−18.90	2.98	8.36	8.78	0.276	8.19 ± 0.14	T_e	LMK03

NOTES.—Col. (1): Galaxy name, ordered by number. Col. (2): Distance modulus. Col. (3): Sech absolute magnitude in K_s. Col. (4): Logarithm of the total H I flux in Jy km s^{-1} based on Gavazzi et al. (2005). Col. (5): Logarithm of the total gas mass in solar masses. Col. (6): Logarithm of the stellar mass in solar masses. Col. (7): Gas fraction. Col. (8): Oxygen abundance and uncertainty. Col. (9): Method of determining abundances: T_e, direct determination via [O III] λ4363 (Osterbrock 1989); R_{23}, determination via the bright line method (McGaugh 1994). Col. (10): Reference for abundances.

REFERENCES.—(V05) this work; (VP03) Vilchez & Iglesias-Paramo 2003; (KS97) Kobulnicky & Skillman 1997; (M97) Martin 1997.

relation using mid-IR luminosities at 4.5 μm from the *Spitzer Space Telescope*. Assuming that most of the galaxies of Salzer et al. (2005) are BCDs and that their total magnitudes approximate the old component, then their results are in agreement with ours, provided BCDs and dIs follow different *L-Z* relations.

The studies quoted in Table 6 may be divided into local and more distant samples of dwarf galaxies. The slopes of the *L-Z* relations for the local samples (Skillman et al. 1989; Richer & McCall 1995; Lee et al. 2003b; Shi et al. 2005; Mendes de Oliveira et al. 2006; Lee et al. 2006; and this work) are all very similar. There may be a difference between the slopes in the blue and infrared, but it is slight. The more distant samples of dwarfs (Lamareille et al. 2004; Tremonti et al. 2004; Salzer et al. 2005), however, all produce *L-Z* relations with steeper slopes, reminiscent

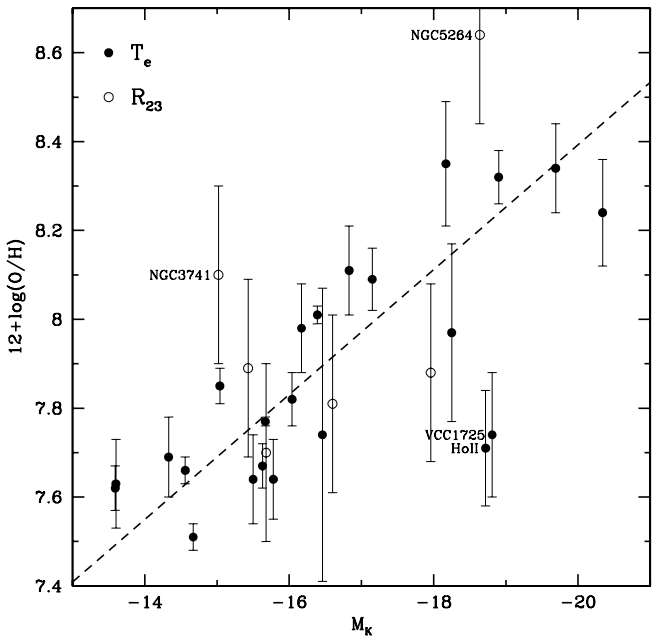

FIG. 5.—Oxygen abundance vs. absolute sech magnitude in K_s for dIs. T_e-based abundances are plotted as filled symbols and R_{23}-based abundances as open symbols. Errors in metallicities are shown as vertical bars. Typical errors for absolute magnitudes are ∼0.1 mag. Four outliers are labeled in the plot. The geometric mean fit to other dIs is plotted as a dashed line.

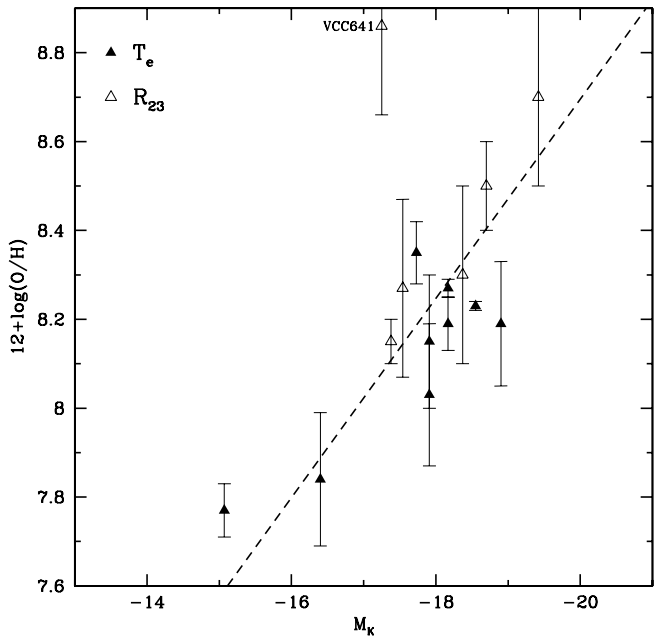

FIG. 6.—Oxygen abundance vs. absolute sech magnitude in K_s for BCDs. T_e-based abundances are plotted as filled symbols and R_{23}-based abundances as open symbols. We include errors in metallicities. Typical errors for absolute magnitudes are ∼0.1 mag. One outlier is labeled. The geometric mean fit to the other BCDs is plotted as a dashed line.

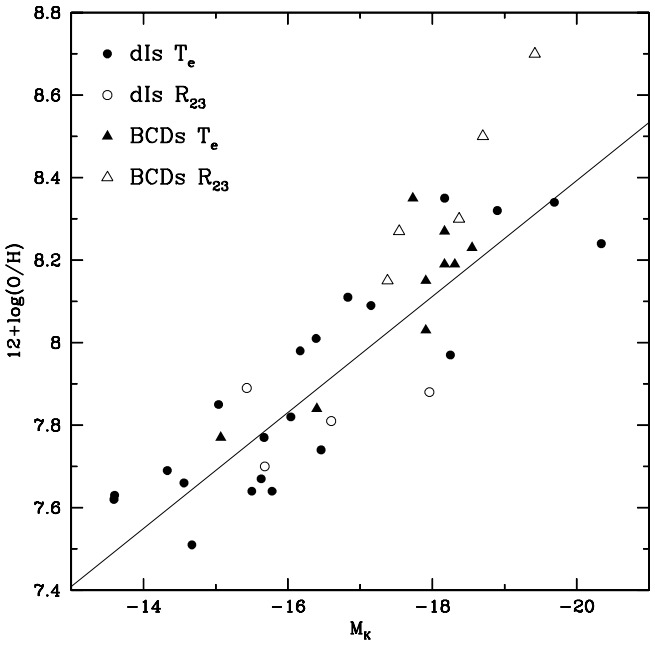

FIG. 7.—Oxygen abundance vs. absolute sech magnitudes in K_s for dIs and BCDs. The dIs are plotted as circles, while BCDs are plotted as triangles. T_e-based abundances are plotted as filled symbols and R_{23}-based abundances as open symbols. The five outliers from Figs. 5 and 6 are not shown. The solid line represents the *L-Z* relation for the dIs.

of our relation for BCDs. If these samples of more distant dwarfs are composed primarily of BCDs with some smaller fractions of dIs, the steeper slopes make sense. However, based on our data, it is possible that the steeper slope arises from an imperfection in the calibration of R_{23} at high metallicity.

5. MASS-METALLICITY RELATIONS

Gas-rich star-forming dwarf galaxies are systems that are well mixed chemically, elemental abundances being observed to vary very little across their faces (Kobulnicky & Skillman 1996, 1997; Pagel 1997), having no significant spacial inhomogeneities in [O III] λ4363 oxygen abundances measured from H II regions located at different galactocentric radii (Lee & Skillman 2004; Lee et al. 2005, 2006b). Chemical evolution can be explored via correlations between oxygen abundance and the stellar mass, gas mass, total mass, and the gas fraction.

Using data in *B* for a sample of dIs observed in the field, Lee et al. (2003b) showed that the oxygen abundance correlates with the stellar mass of the systems. However, in another sample of dIs in the Virgo Cluster, the relation was more scattered. Lee et al. (2003c) found also that the relation with the gas mass was scattered for the field sample, and that some Virgo dIs were depleted in gas. The relation between metallicity and the gas fraction suggested that the evolution of some dIs in Virgo was affected by flows, such as stripping of gas due to the cluster neighborhood. The authors showed that this relationship could be used unequivocally to recognize gas deficiency in dwarfs. Below we address the relations between metallicity and mass, employing NIR photometry.

5.1. *Gas Masses*

The total mass of gas can be gauged from the H I 21 cm flux, F_{21}, measured by radio observations (Huchtmeier et al. 2000, 2001, 2003). Data for dIs are summarized by Karachentsev et al. (2004). We include in Table 4 the logarithm of the total H I flux from the latter source. For Virgo BCDs, H I fluxes are given in Table 5. They are derived from Gavazzi et al. (2005), who synthesize a set of data for 355 late-type galaxies in the Virgo cluster with H I masses for many dwarfs derived from previous work by Hoffman and collaborators (Huchtmeier et al. 2000, 2001, 2003).

The H I mass, $M_{\rm H\,I}$, in solar masses is given by the following equation (Roberts 1975; Roberts and Haynes 1994):

$$M_{\rm H\,I} = 2.356 \times 10^5 F_{21} D^2, \quad (5)$$

TABLE 6
LUMINOSITY-METALLICITY RELATIONS FOR STAR-FORMING GALAXIES

Band (1)	Sample (2)	*L-Z* Slope (3)	*L-Z* Intercept (4)	rms (5)	Reference (6)
B	19 dIs	−0.153	5.500	0.16	SKH89
B	12 dIs	−0.147 ± 0.029	5.670 ± 0.480	0.09	RM95
B	22 dIs	−0.153 ± 0.025	5.590 ± 0.540	0.17	LMK03
B	21 dIs	−0.149 ± 0.011	5.650 ± 0.170	0.15	ZH06
B	×100 MP SFGs from 2dFGRS	−0.200 ± 0.020	4.290 ± 0.420	>0.3	LMC04
B	6387 SFGs from 2dFGRS	−0.223 ± 0.004	4.070 ± 0.090	0.32	LMC04
B	∼53000 SFGs from SDSS	−0.185 ± 0.001	5.238 ± 0.018	>0.3	THK04
B	24 dwarf BCGs $M_B > -18$	−0.139 ± 0.011	5.800 ± 0.170	>0.2	SKL05
B	48 BCGs $M_B < -18$	−0.079 ± 0.018	6.930 ± 0.370	>0.2	SKL05
B	765 SFGs from KISS	−0.222 ± 0.003	4.180 ± 0.060	0.25	SLM05
J	420 SFGs from KISS	−0.200 ± 0.004	4.130 ± 0.090	0.22	SLM05
K	370 SFGs from KISS	−0.195 ± 0.004	4.030 ± 0.010	0.23	SLM05
K	29 dwarfs from Paper I and 2MASS	−0.140 ± 0.020	5.550 ± 0.260	0.15	O06
J	25 dIs	−0.140 ± 0.014	5.692 ± 0.214	0.11	V05
K	25 dIs	−0.141 ± 0.015	5.581 ± 0.244	0.10	V05
J	14 BCDs	−0.216 ± 0.027	4.530 ± 0.473	0.12	V05
K	14 BCDs	−0.224 ± 0.030	4.212 ± 0.537	0.11	V05

NOTES.—Col. (1): Observing band (for the absolute magnitude). Col. (2): Sample: SFGs, star-forming galaxies; BCGs, blue compact galaxies; MP, metal-poor [12 + log (O/H) ≲ 8.3]. Col. (3): *L-Z* relation slope. Col. (4): *L-Z* relation intercept. Col. (6): rms error in log (O/H). Col. (5): Reference.

REFERENCES.—(SKH89) Skillman et al. 1989; (RM95) Richer & McCall 1995; (LMK03) Lee et al. 2003b; (ZH06) van Zee & Haynes 2006; (LMC04) Lamareille et al. 2004; (THK04) Tremonti et al. 2004; (SKL05) Shi et al. 2005; (SLM05), Salzer et al. 2005; (O06) Mendes de Oliveira et al. 2006; (V05) Vaduvescu 2005 or this work.

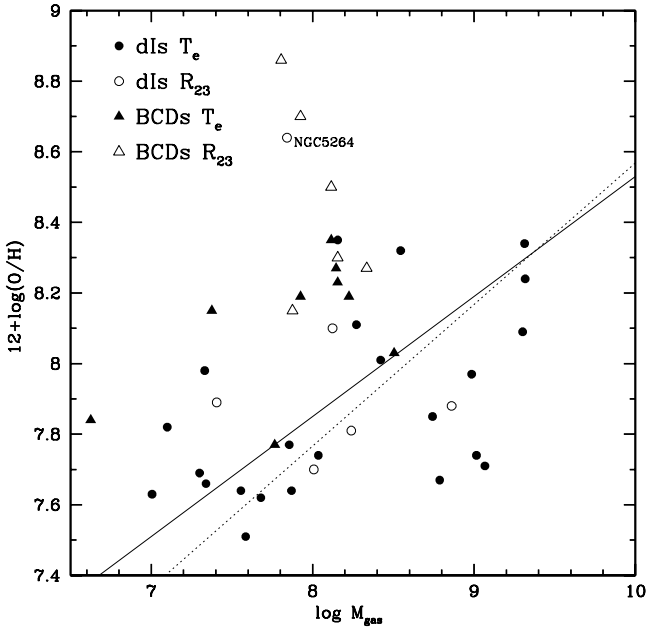

FIG. 8.—Correlation between oxygen abundance and the gas mass. The dIs are plotted with circles and BCDs with triangles. T_e-based abundances are plotted as filled symbols and R_{23}-based abundances as open symbols. The dIs with a greater gas mass are more abundant in metals. Ignoring NGC 5264, the geometric linear fit to the dI data is marked by a solid line. For comparison, the fit found by Lee et al. (2003b) is shown with a dotted line. BCDs often have less gas than dIs at a given metallicity.

where F_{21} is the 21 cm flux integral in Jy km s^{-1} and D is the distance in megaparsecs. To account for helium and other metals, the total gas mass in solar masses is given by

$$M_{\rm gas} = M_{\rm H\,I}/X, \tag{6}$$

where X is the fraction of the gas in the form of hydrogen, here assumed to be 0.733 (Lee et al. 2003b). In Table 4 we include the logarithm of the total gas mass for the dIs in our sample, calculated from F_{21} and the distance modulus included in the first column. In Table 5 we include the logarithm of the total gas mass for the BCDs in our sample.

Figure 8 plots the metallicity versus the logarithm of the total gas mass (expressed in solar units). The dIs are plotted with circles, and BCDs with triangles. Dwarfs having T_e abundances are plotted with filled symbols and those having R_{23} abundances with open symbols. The correlation for the dIs is very poor, with NGC 5264 again being an outlier in the sample. Rejecting this point, a geometric linear fit to the rest of the dI sample (28 objects) gives the following relation:

$$12 + \log({\rm O/H}) = (5.13 \pm 0.45) + (0.34 \pm 0.06)\log(M_{\rm gas}). \tag{7}$$

This relation is very close to the fit found by Lee et al. (2003b), who used data for 21 dIs. The two samples overlap, with the sample of Lee et al. (2003b) extending from $M_B = -18$ to -11 mag (corresponding to M_K from -21 to -14), and our sample extending from $M_K = -20$ to -13. We plot in Figure 8 our fit with a solid line and the fit of Lee et al. (2003b) with a dotted line. Some Virgo BCDs lie leftward of the dI envelope, i.e., less gas for a given oxygen abundance, a result found also in Lee et al. (2003c) for their Virgo dI sample, suggesting that they are depleted in gas relative to dIs of comparable metallicity. Either they are less massive systems overall, or gas has been removed, perhaps by dynamical interactions in the cluster environment.

5.2. *Stellar Masses*

In Paper I it was shown that the shape of the unresolved (diffuse) stellar component of nearby dIs in the NIR is approximated well by a hyperbolic secant (sech) function. In Paper II it was demonstrated that the same function fits the shape of the diffuse component underlying star formation bursts in BCDs. It is believed that the luminosity associated with the sech model provides a good estimate of the contribution to the light by stellar populations older than about 3 Gyr (Paper I). As such, it should be the best gauge of total stellar mass.

Expressed in solar masses, stellar masses can be calculated from

$$\log M_* = \log\frac{M_*}{L_K}({\rm old}) - 0.4[M_K({\rm old}) - M_{K\odot}], \tag{8}$$

where M_*/L_K(old) is the mass-to-light ratio of the old stellar component in K_s, in solar units, M_K(old) is the absolute magnitude of the old component in K_s, and $M_{K\odot}$ is the absolute magnitude of the Sun in K_s. Here we prefer the sech magnitudes derived in Papers I and II as representative of the luminosity of the old population, M_K(old). However, we augment the dI sample with galaxies detected by 2MASS for which cataloged total magnitudes are used as estimates of M_K(old). These galaxies are distinguished symbolically in plots. For the absolute magnitude of the Sun, we adopt $M_{K\odot} = +3.3$ (Bessell et al. 1998).

For low-metallicity galaxies (0.004–0.0004 $Z_\odot$), L. Portinari (2005, private communication) derived $M_*/L_K \sim 0.8\ M_\odot/L_{K\odot}$ using population synthesis models. Drory et al. (2004) obtained an identical result from composite stellar population models for ages between about 4 and 8 Gyr (see their Fig. 1). From extensive modeling of the Milky Way, Bissantz et al. (2003) derived $M_*/L_K = 0.6$. Based on galaxy evolution models to investigate the relation between mass-to-light ratios and colors of spiral galaxies, de Jong & Bell (2003) predict $M/L_K \sim 1\ M_\odot/L_{K\odot}$ for $B - R \sim 2$ mag (which can be regarded as an average color of dwarfs). Here, we adopt $M_*/L_K = 0.8\ M_\odot/L_{K\odot}$.

5.3. *Baryonic Masses*

Assuming baryonic matter consists of gas and stars only, the baryonic mass of a galaxy can be expressed simply by the sum of the two components, $M_{\rm bary} = M_{\rm gas} + M_*$. Figure 9 plots the metallicity versus the logarithm of the baryonic mass expressed in solar masses. The dIs are plotted with circles, and BCDs with triangles. Dwarfs having T_e abundances are plotted with filled symbols, while those having R_{23} abundances with open symbols. In the dI sample, NGC 5264 is once more an outlier. Rejecting this point, a geometric linear fit to the rest of the sample (28 dIs) gives the following relation:

$$12 + \log({\rm O/H}) = (4.91 \pm 0.46) + (0.35 \pm 0.05)\log\left(M_{\rm bary}\right). \tag{9}$$

This relation is very close to the fit found by Lee et al. (2003b), which was derived from B photometry for 21 dIs in the field. We plot our fit with a solid line and the fit of Lee et al. (2003b) with a dotted line. The close agreement suggests that the two-component decomposition scheme of Lee et al. (2003b) was effective for deriving stellar masses. Most BCDs in Figure 9 appear to lie at lower baryonic masses compared to dIs at a given oxygen abundance,

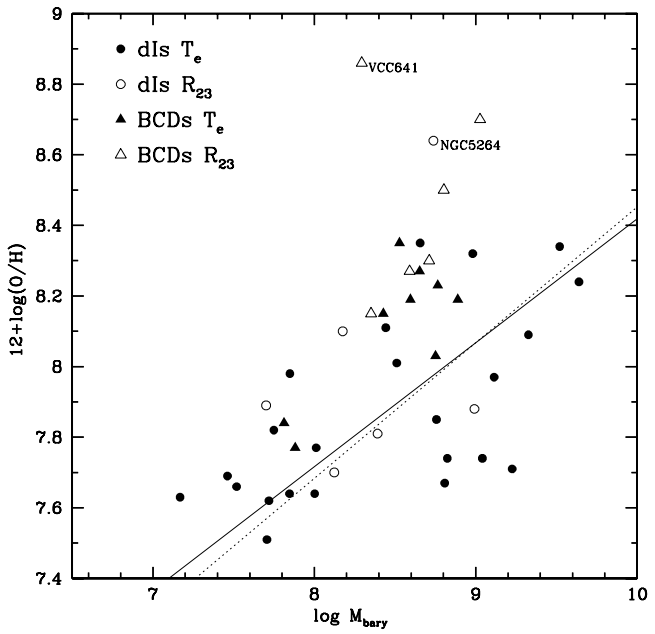

FIG. 9.—Correlation between oxygen abundance and baryonic mass. The dIs are plotted with circles and BCDs with triangles. T_e-based abundances are plotted as filled symbols and R_{23}-based abundances as open symbols. Stellar masses were derived from sech magnitudes in K_s. More massive dIs are more abundant in metals. Ignoring NGC 5264, the geometric linear fit to the dI data is drawn as a solid line. For comparison, the Lee et al. (2003b) fit is plotted with a dashed line.

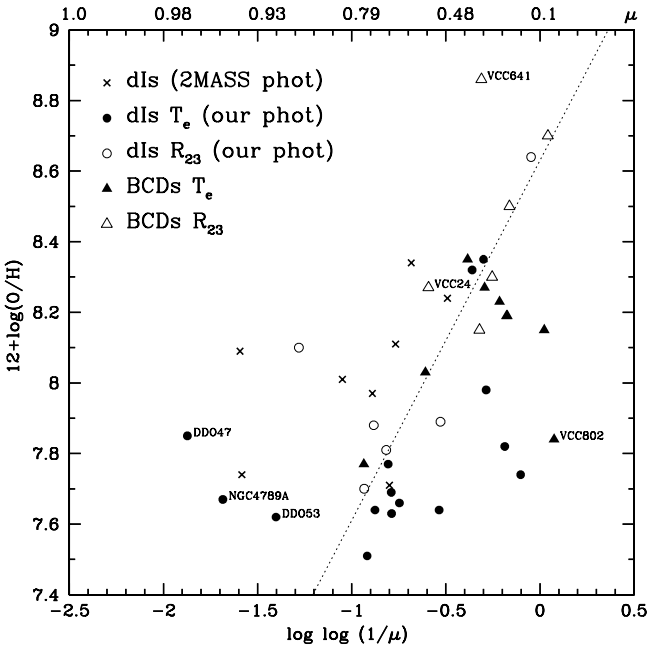

FIG. 10.—Correlation between oxygen abundance and the gas fraction, μ. The dIs whose stellar masses were derived from sech magnitudes in K_s (Paper I) are plotted with circles, and those derived from 2MASS photometry are plotted with crosses. BCDs, all of whose stellar masses were derived from sech magnitudes in K_s, are represented with triangles. T_e-based abundances are plotted as filled symbols and crosses, and R_{23}-based abundances are plotted as open symbols. The linear fit derived by Lee et al. (2003b) for his field dI sample is plotted with a dotted line. The gas fraction increases toward the left. Although there is a lot of scatter, most dIs and BCDs appear to follow the closed box model.

possibly as a consequence of how BCDs are selected. It is possible that larger galaxies with comparable bursts are simply not classified as BCDs!

5.4. *Metallicity and Gas Fraction*

The closed box model of chemical evolution predicts a linear correlation between $n(\mathrm{O})/n(\mathrm{H})$ and the logarithm of the inverse gas fraction $1/\mu$, where

$$\mu = \frac{M_{\mathrm{gas}}}{M_{\mathrm{gas}} + M_*}. \tag{10}$$

The slope of the relation conveys the yield of oxygen. Judging stellar masses from BV photometry, Lee et al. (2003b) concluded that field dIs obey the closed box model, implying that their evolution has been isolated. Here we study the correlation obtained for both dIs and BCDs using NIR sech luminosities to assess stellar masses. In principle, our masses should be more reliable, as they are less sensitive to recent star formation.

Figure 10 plots log (O/H) versus log [log $(1/\mu)$], for which the closed box model predicts a linear correlation with a slope of unity and an intercept equal to the yield. Gas fraction μ increases to the left, according to the labels plotted along the top horizontal axis. We represent dIs with photometry from the present work with circles, and dIs with 2MASS photometry with crosses. We plot the fit of Lee et al. (2003b) with a dotted line. Most dIs from our sample lie close to the fit of Lee. We overlay in Figure 10 triangles representing our BCD sample. Most BCDs appear close to the fit of Lee, too, with about three outliers. Note that gas has not been detected in VCC 802, so its abscissa is a lower limit. One possibility is that VCC 802 has been stripped due to the hot intracluster medium, since it is projected near the M86/M84 clump, which is a region of enhanced density (Boehringer et al. 1994). If dIs follow the closed box model, as the data suggest, then the proximity of BCDs to the dI locus suggests that bursts in present-day BCDs do not have sufficient strength to blow out neutral gas from the host galaxies. The fact that several dIs and at least one BCD do show H I deficiencies in dense environments (Lee et al. 2003b; this paper) indicates that external processes are more likely to remove gas from dwarfs. In summary, we concur with Lee that the evolution of field dIs has not been affected much by flows. We also conclude that BCDs have evolved similarly to dIs.

6. IMPLICATIONS FOR EVOLUTION

A few evolutionary scenarios that involve dIs and BCDs have been proposed over the years, most without firm conclusions (e.g., Papaderos et al. 1996b). Some links have emerged using stellar masses derived from data in the visible, although with large scatter. We summarize below our main results.

For both dIs and BCDs, metallicity correlates with stellar mass, gas mass, and baryonic mass, in the sense that more massive systems are more enriched in metals. Our most important discovery is that the relationship between the metallicity and the gas fraction for BCDs follows that for dIs. It means that BCDs and dIs have evolved similarly. Using NIR photometry, we confirm the conclusion of Lee et al. (2003b) that the evolution of field dIs has not been noticeably influenced by gas flows. By implication, the same conclusion must be reached for BCDs. Thus, star formation bursts in BCDs are unlikely to be caused by the transfer of material from elsewhere.

7. CONCLUSIONS

Oxygen abundances have been derived for four blue compact dwarf galaxies in the Virgo Cluster observed in a queue run at Gemini North in 2003. Drawing on the NIR properties studied in Papers I and II and oxygen abundances from our work and the

literature, we studied the correlations between the metallicity and the stellar mass, gas mass, baryonic, mass, and the gas fraction for both dIs and BCDs. Metallicity correlates with all four parameters, in the sense that more massive systems contain more metals. The oxygen abundance correlates well with the luminosity in K_s, for both dIs and BCDs. Using NIR sech magnitudes to measure luminosity, the L_K-Z relations for dIs and BCDs are statistically indistinguishable. The dIs and BCDs appear to share a common relationship between metallicity and the gas fraction, namely, one which is consistent with closed box evolution. Thus, BCDs appear to be dIs with enhanced star formation activity. The origin of the enhancement remains unknown, but it is unlikely to be caused by flows.

We thank the Gemini North time allocation committees for granting us the opportunity to observe. M. L. M. thanks the Natural Sciences and Engineering Research Council of Canada for its continuing support. M. G. R. acknowledges financial support from CONACyT grant 43121 and UNAM DGAPA grants IN108406-2, IN108506-2, and IN112103. O. V. thanks Henry Lee for providing up-to-date references regarding metallicities. Special acknowledgement is due to Jose Manuel Vilchez, who served as the external examiner for the Ph.D. thesis of O. V., providing interesting discussions. Thanks are due to Robin Fingerhut for providing updated distances of dwarfs in the Local Volume. For our data reductions, we used the GEMINI package written at the Gemini Observatories and IRAF, which is maintained by the National Optical Astronomy Observatory, operated by the Association of Universities for Research in Astronomy, Inc., under cooperative agreement with the National Science Foundation. This research has made use of the GOLDMine Database in Milano and the NASA/IPAC Extragalactic Database (NED), which is operated by the JPL, CALTECH, under contract with NASA. Special acknowledgement is due to the anonymous referee, who provided discussions which allowed us to improve the manuscript.

REFERENCES

Allende Prieto, C., Lambert, D. L., & Asplund, M. 2001, ApJ, 556, L63
Bessell, M. S., Castelli, F., & Plez, B. 1998, A&A, 333, 231
Binggeli, B. 1994, in Dwarf Galaxies, ed. G. Meylan & P. Prugniel (Garching: ESO), 13
Bissantz, N., Englmaier, P., & Gerhard, O. 2003, MNRAS, 340, 949
Boehringer, M., Briel, U. G., Schwarz, R. A., Voges, W., Hartner, G., & Trumper, J. 1994, Nature, 368, 828
de Jong, R. S., & Bell, E. F. 2003, in The Mass of Galaxies at Low and High Redshift, ed. R. Bender & A. Renzini (Berlin: Springer), 213
Draper, N. R., & Smith, H. 1998, Applied Regression Analysis (New York: Wiley)
Drory, N., Bender, R., Feulner, G., Hopp, U., Maraston, C., Snigula, J., & Hill, G. J. 2004, ApJ, 608, 742
Fitzpatrick, E. L. 1999, PASP, 111, 63
Gallagher, G., & Hunter, D. A. 1989, AJ, 98, 806
Garnett, D. R. 2002, ApJ, 581, 1019
Gavazzi, G., Boselli, A., van Driel, W., & O'Neil, K. 2005, A&A, 429, 439
Grebel, E. K. 2001a, in ASP Conf. Ser. 239, Microlensing 2000: A New Era of Microlensing Astrophysics, ed. J. W. Menzies & P. D. Sackett (San Francisco: ASP), 280
———. 2001b, Ap&SS Suppl., 277, 231
Guseva, N. G., Izotov, Y. I., & Thuan, T. X. 2000, ApJ, 531, 776
Helmi, A., et al. 2006, ApJ, 651, L121
Hodge, P., & Miller, B. W. 1995, ApJ, 451, 176
Huchtmeier, W. K., Karachentsev, I. D., & Karachentseva, V. E. 2001, A&A, 377, 801
———. 2003, A&A, 401, 483
Huchtmeier, W. K., Karachentsev, I. D., Karachentseva, V. E., & Ehle, M. 2000, A&AS, 141, 469
Izotov, Y. I., & Thuan, T. X. 1999, ApJ, 511, 639
James, P. A. 1994, MNRAS, 269, 176
Karachentsev, I. D., Karachentseva, V. E., Huchtmeier, W. K., & Makarov, D. I. 2004, AJ, 127, 2031
Kauffmann, G., White, S. D. M., & Guiderdoni, B. 1993, MNRAS, 264, 201
Kennicutt, R. C., & Skillman, E. D. 2001, AJ, 121, 1461
Kobulnicky, H. A., & Skillman, E. D. 1996, ApJ, 471, 211
———. 1997, ApJ, 489, 636
Krawchuk, C. A. P., McCall, M. L., Komljenovic, M., Kingsburgh, R., Richer, M., & Stevenson, C. 1997, in IAU Symp. 180, Planetary Nebulae, ed. H. J. Habing &, G. L. M. Lamers (Dordrecht: Kluwer), 116
Kunth, D., & Ostlin, G. 2000, A&A Rev., 10, 1
Lamareille, F., Mouhcine, M., Contini, T., Lewis, I., & Maddox, S. 2004, MNRAS, 350, 396
Lee, H., Grebel, E. K., & Hodge, P. W. 2003a, A&A, 401, 141
Lee, H., McCall, M. L., Kingsburgh, R. L., Ross, R., & Stevenson, C. 2003b, AJ, 125, 146
Lee, H., McCall, M. L., & Richer, M. G. 2003c, AJ, 125, 2975
Lee, H., & Skillman, E. D. 2004, ApJ, 614, 698
Lee, H., Skillman, E. D., Cannon, J. M., Jackson, D. C., Gehrz, R. D., Polomski, E. F., & Woodward, C. E. 2006a, ApJ, 647, 970
Lee, H., Skillman, E. D., & Venn, K. A. 2005, ApJ, 620, 223
———. 2006b, ApJ, 642, 813
Lee, J., Salzer, J. J., & Melbourne, J. 2004, ApJ, 616, 752
Lequeux, J., Peimbert, M., Rayo, J. F., Serrano, A., & Torres-Peimbert, S. 1979, A&A, 80, 155
Martin, C. L. 1997, ApJ, 491, 561
Mateo, M. 1998, ARA&A, 36, 435
Matthews, L. D., & Gallagher, J. S. 1997, AJ, 114, 1899
McCall, M. L., Rybski, P. M., & Shields, G. A. 1985, ApJS, 57, 1
McGaugh, S. S. 1991, ApJ, 380, 140
———. 1994, ApJ, 426, 135
Melbourne, J., Phillips, A. S., John, J., Gronwall, C., & Sarajedini, V. L. 2004, AJ, 127, 686
Melbourne, J., & Salzer, H. J. 2002, AJ, 123, 2302
Mendes de Oliveira, C. L., Temporin, S., Cypriano, E. S., Plana, H., Amram, P., Sodre, L., Jr., & Balkowski, C. 2006, AJ, 132, 570
Miller, B. W., & Hodge, P. 1996, ApJ, 458, 467
Moles, M., Aparicio, A., & Masegosa, J. 1990, A&A, 228, 310
Osterbrock, D. E. 1989, Astrophysics of Gaseous Nebulae and Active Galactic Nuclei (Mill Valley: University Science Books)
Pagel, B. E. J. 1997, Nucleosynthesis and the Chemical Evolution of Galaxies (Cambridge: Cambridge Univ. Press)
Pagel, B. E. J., Edmunds, M. G., Blackwell, D. E., Chun, M. S., & Smith, G. 1979, MNRAS, 189, 95
Papaderos, P., Loose, H.-H., Fricke, K. J., & Thuan, T. X. 1996b, A&A, 314, 59
Papaderos, P., Loose, H.-H., Thuan, T. X., & Fricke, K. J. 1996a, A&AS, 120, 207
Peimbert, M., Peimbert, A., Esteban, C., Garcia-Rojas, J., Bresolin, F., Carigi, L., Ruiz, M. T., & Lopez-Sanchez, A. R. 2007, Rev. Mex. AA Ser. Conf., in press (astro-ph/0608440)
Richer, M. G., & McCall, M. L. 1995, ApJ, 445, 642
Roberts, M. S. 1975, in Radio Observations of Neutral Hydrogen in Galaxies, in Galaxies and the Universe, ed. A. Sandage, M. Sandage, & J. Kristian (Chicago: Univ. Chicago Press), 309
Roberts, M. S., & Haynes, M. P. 1994, ARA&A, 32, 115
Salzer, J. J., Lee, J. C., Melbourne, J., Hinz, J. L., Alonso-Herrero, A., & Jangren, A. 2005, ApJ, 624, 661
Saviane, I., Held, E. V., Ivanov, V., Alloin, D., Bresolin, F., Rich, R. M., Rizzi, L., & Momany, Y. 2005, in IAU Colloq. 198, Near-Field Cosmology with Dwarf Elliptical Galaxies, ed. H. Jerjen & B. Binggeli (Cambridge: Cambridge Univ. Press), 202
Searle, L., & Sargent, W. L. W. 1972, ApJ, 173, 25
Shi, F., Kong, X., Li, C., & Cheng, F. Z. 2005, A&A, 437, 849
Skillman, E. D., Kennicutt, R. C., & Hodge, P. W. 1989, ApJ, 347, 875
Skillman, E. D., Televich, R. J., Kennicutt, R. C., Garnett, D. R., & Terlevich, E. 1994, ApJ, 431, 172
Sparke, L., & Gallagher, J. S. 2000, Galaxies in the Universe: An Introduction (Cambridge: Cambridge Univ. Press)
Stasinska, G., Comte, G., & Vigroux, L. 1986, A&A, 154, 352
Stavely-Smith, L., Davies, R. D., & Kinman, T. D. 1992, MNRAS, 258, 334
Tammann, G. A. 1994, in Dwarf Galaxies, ed. G. Meylan & P. Prugniel (Garching: ESO), 3
Thuan, T. X. 1985, ApJ, 299, 881
Tremonti, C. A., et al. 2004, ApJ, 613, 898
Tully, R. B., Boesgaard, A. M., Dyck, H. M., & Schempp, W. V. 1981, ApJ, 246, 38

Vaduvescu, O. 2005, Ph.D. thesis, York Univ.
Vaduvescu, O., McCall, M. L., Richer, M. G., & Fingerhut, R. L. 2005, AJ, 130, 1593 (Paper I)
Vaduvescu, O., Richer, M. G., & McCall, M. L. 2006, AJ, 131, 1318 (Paper II)
van den Bergh, S. 2000, The Galaxies of the Local Group (Cambridge: Cambridge Univ. Press)
van Zee, L., & Haynes, M. P. 2006, ApJ, 636, 214
van Zee, L., Haynes, M. P., & Salzer, J. J. 1997, AJ, 114, 2497
van Zee, L., Skillman, E., & Haynes, M. P. 2006, ApJ, 637, 269
Venn, K. A., Irwin, M., Shetrone, M. D., Tout, C. A., Hill, V., & Tolstoy, E. 2004, AJ, 128, 1177
Vilchez, J. M., & Iglesias-Paramo, J. 2003, ApJS, 145, 225
Webster, B. L., & Smith, M. G. 1983, MNRAS, 204, 743
White, S. D. M., & Frenk, C. S. 1991, ApJ, 379, 52